İSTANBUL UNIVERSITY CERRAHPAŞA

ORIGINAL ARTICLE
Electrica 2024; 24(1): 39-50

Stabilizing and Control of the DC-Microgrid Systems with PV Panels and CPLs

Hossein Akbari, Jalal Nazarzadeh

Department of Electric Power Engineering, Shahed University Faculty of Engineering, Tehran, Iran

Cite this article as: H. Akbari and J. Nazarzadeh, "Stabilizing and control of the DC-microgrid systems with PV panels and CPLs," *Electrica*, 24(1), 39-50, 2024.

ABSTRACT

The DC/DC converters are commonly used in DC microgrids to achieve the desired performance of a system under different operating conditions. The dynamics of an isolated DC microgrid with solar photovoltaic panels, battery, and constant power load is a fractional nonlinear model; thus, the complex nonlinear method should be applied for controller design and stabilizing the system. In multi-input multi-output systems with non-linear elements, non-linear control methods should be used, but this paper presents a straightforward technique for designing decentralized controllers for the buck, boost, and buck-boost converters in an isolated DC microgrid to stabilize the system and Maximum Power Point Tracking (MPPT) control of the solar photovoltaic panels. The presented methods can consider the nonlinear decentralized feedback linearizing control for the nonlinear system. Depending on the performance of the converters in the system, proper dynamic models are introduced for the converters, and decentralized controllers are determined. Various scenarios are simulated and compared to conventional methods. The results indicate that the settling time of the output variables and the overvoltage of the DC-link voltage are reduced by less than 30% compared to other techniques.

Index Terms— Constant Power Loads, DC/DC converters, isolated DC microgrid

I. INTRODUCTION

With the increasing penetration of new energy sources, microgrids are a great alternative to existing networks. Compared to alternating current (AC) microgrids, direct current (DC) microgrids have the advantages of good power quality, simple integration with energy storage, good compatibility with consumer electronics, ease of control, availability, and higher reliability [1, 2]. These benefits, along with the features of no need for synchronization and frequency control, elimination of reactive power, and harmonic issues, make DC microgrids a "return to Edison" phenomenon [3, 4]. In contrast, the operation of isolated direct current microgrid (IDCM) with distributed generation (DG) sources, energy storage, and nonlinear loads have challenges such as difficulty in achieving voltage regulation, power sharing, and potential instability (destabilizing negative impedance characteristics) due to constant power load (CPL) [5]. The IDCMs face the challenge of instability due to nonlinear devices such as photovoltaic (PV) arrays, CPLs, and low inertia. Therefore, designing decentralized controllers to stabilize IDCMs with CPLs is a common problem [6].

In this regard, one of the common methods of controlling DC microgrids is the hierarchical control method [7]. Hierarchical control can be divided into primary, secondary, and tertiary controls. The primary control is used to control the load sharing between the DGs; the secondary control is responsible for regulating the voltage fluctuation; and the third control is considered for regulating the power-sharing between the DC microgrid and the upstream network. A droop controller can be used to achieve power sharing at the primary level. However, droop controllers have line impedance problems in large-scale DC microgrids and current sharing [8]. Also, conventional droop controllers cannot accurately share the current between different sources. Hence, an improved droop controller has been investigated to enhance the current sharing performance[9].

AC microgrids' hierarchical and fuzzy control methods are more complex and less reliable than IDCMs [10, 11]. On the other hand, the nonlinear controllers in the IDCMs require a careful nonlinear analysis of the system [12]. In this regard, the backstepping algorithm can cause steady-state

Corresponding author:
Jalal Nazarzadeh

E-mail:
nazarzadeh@shahed.ac.ir

Received: January 12, 2023

Revision Requested: February 28, 2023

Last Revision Received: July 12, 2023

Accepted: August 19, 2023

Publication Date: January 5, 2024

DOI: 10.5152/electrica.2024.23002

tracking errors because it does not directly deal with output voltage regulation [13]. Although a nonlinear controller based on differential geometry theory can be connected to an IDCM, this method cannot guarantee the system's stability [14]. Also, the choice of the slide level, dependence on load, and chattering can be considered sliding mode control problems in stabilizing an IDCM [15]. Droop-based primary controllers are faced with a trade-off between voltage regulation and load-sharing accuracy [16].

On the other hand, due to the complexity of the decentralized controllers proposed, it will be challenging to extend to other IDCMs [17]. A class of IDCM has been studied based on passivity theory with a non-affine dynamical model, and a centralized controller in the system has been designed [18-20]. Although this controller can be designed based on the affine system in the IDCM, its implementation is complex [21]. Moreover, the current–voltage state-space models of the converters with the CPLs appear in the nonlinear fractional terms in the dynamical models of the IDCM. In this case, because the variations of the CPLs are considered an independent disturbance of the system, this disturbance does not have sufficient accuracy in modeling the CPLs [22]. The state-space models of DC/DC converters with energy variables can be used to design the conventional controllers in an IDCM with CPLs [23]. This approach provides a suitable space for implementing closed-loop classical controllers and achieves the desired performances.

Other control techniques, such as fuzzy-sliding control with an observer [24] and adaptive backstepping sliding mode control [25], have been proposed for a DC/DC boost converter and CPL. Also, in [26], modular controllers based on small signal stability analysis have been suggested for an IDCM with CPL. Despite introducing different control techniques, the decentralized controllers in an IDCM with different types of DC/DC converters, CPL, and MPP control would be significant if they provide modular implementation and stability in nonlinear conditions.

This article introduces the proper average models of DC/DC converters based on special variables in an IDCM, incorporating a solar PV panel, a storage system, and CPL. Also, three decentralized controllers are designed by applying the nonlinear feedback linearization technique for buck, boost, and buck-boost converters in an IDCM. These controllers provide complete stability for the IDCM at all operating points. In addition, the dynamic performances of the proposed controllers are obtained and compared with other conventional and modern methods, and their capabilities are evaluated.

A comparison between different techniques for controlling an IDCM is summarized in Table I. This comparison is based on various indices, including modular implementation, considering constant power load, nonlinear stability analysis, and considering multiple DC/DC converters.

The present article is organized into the following sections. In the first section, nonlinear models of DC/DC converters are introduced and augmented in an IDCM. In the continuation, structures of the closed-loop controllers for different DC/DC converters are introduced, and decentralized controllers based on system parameters are determined. Finally, the performance of conventional, passive, and proposed controllers is demonstrated and evaluated together.

TABLE I. A COMPARISON BETWEEN SOME PREVIOUS STUDIES WITH PROPOSED TECHNIQUE FOR CONTROL OF AN ISOLATED DC MICROGRID

	Comparison Items				
Reference	**MI**	**CPL**	**NSA**	**MC**	**Key Future**
[8]	×	×	×	×	Hierarchical power sharing.
[9]	×	×	×	×	Droop control with active disturbance.
[12]	✓	×	✓	✓	Voltage control by nonlinear technique.
[13]	×	✓	✓	×	Voltage control by H_∞ approach.
[17]	✓	✓	✓	×	Voltage control by high gain observer.
[18]	×	×	✓	✓	Voltage control by passivity theory.
[24]	×	✓	✓	×	Voltage control by fuzzy-sliding control.
[25]	×	✓	✓	×	Adaptive backstepping sliding control.
[26]	✓	✓	×	×	Modular controller by small signal model.
proposed controller	✓	✓	✓	✓	Voltage control by feedback linearization.

CPL, constant power load; MC, multi-DC/DC converters; MI, modular implementation; NSA, nonlinear stability analysis.

II. ISOLATED DIRECT CURRENT MICROGRID STRUCTURE

Fig. 1 shows the structure of an IDCM. The DC/DC boost converter on the PV side is controlled to extract the maximum available power from the solar PV panels in the form of the Maximum Power Point Tracking (MPPT) unit. The role of the MPPT algorithm is to keep the operating point of the solar module at the MPP of the *I–V* curve [12]. A bidirectional DC/DC buck-boost converter is connected to the battery to regulate the DC-link voltage when the PV operating point is changed. The IDCM in Fig. 1 consists of a DC/DC buck converter. This converter is connected to the DC-link capacitor from a long transmission line with dc resistance R_L and adjusts the CPL voltage. The main source of input energy for the IDCM in Fig. 1 is a solar PV panel. A solar cell can be represented as part of an electrical circuit with a p–n junction modeled by a diode and a photocurrent generator. Also, the solar PV panel generates current from radiation, and two series and parallel resistances are considered for presenting the Joule effect and recombination losses. This compound is called the single-diode solar cell model. A circuit model of a solar PV cell is shown in Fig. 2 with single-diode, series, and parallel resistances [27]. The parallel resistance () indicates leakage through the p–n junction of the PV cell, and the series resistance (R_s) indicates the electrical losses of the cell surface and size.

Also, the solar PV panel generates current from radiation, and two series and parallel resistances are considered for presenting the Joule effect and recombination losses. This compound is called the single-diode solar cell model. A circuit model of a solar PV cell is shown in Fig. 2 with single-diode, series, and parallel resistances [27].

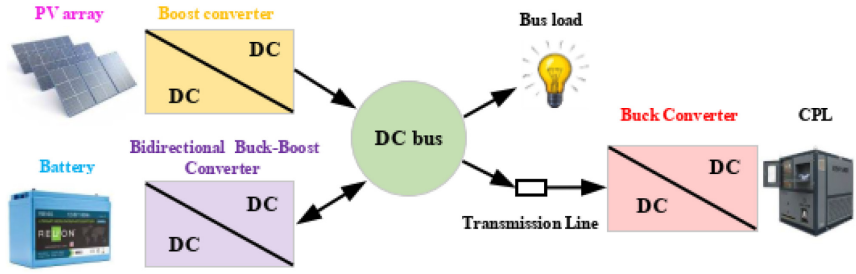

Fig. 1. Structure of the isolated direct current microgrid

The parallel resistance (R_p) indicates leakage through the p–n junction of the PV cell, and the series resistance (R_s) indicates the electrical losses of the cell surface and size.

For an ideal PV cell, the series and shunt resistances are zero and infinite, respectively. In Fig. 2, the current source (i_{ph}) is dependent on sunlight and ambient temperature. The output current of the PV array (i_p) is

$$i_p = i_{ph} - I_o\left(e^{\alpha(v_1+R_s i_p)}-1\right)-\frac{v_1+R_s i_p}{R_p} \tag{1}$$

where $\alpha = q/(N_s kT)$, and v_1 and I_o are the PV output voltage and reverse saturation current of the diode. Also, q , k , T , and N_s are the electron charge, Boltzmann's constant, the cell temperature, and the number of series cells, respectively.

The photocurrent (i_{ph}) is linearly dependent on solar radiation (G) and is also affected by PV temperatures.

$$i_{ph} = \frac{G}{G_{ref}}\left(I_{pvn} + K_i\left(T_0 - T_r\right)\right) \tag{2}$$

where I_{pvn} , K_i , and T_r are the produced nominal photocurrent, the temperature coefficient of the short circuit current of the solar PV panel, and the reference temperature 25° C, respectively. Also, G_{ref} and T_0 are the reference radiation $1000w/m^2$ and the ambient temperature. Fig. 2-b shows the characteristic curves $i_p - v_1 \& p_p - v_1$ of a typical solar PV panel. At the MPP, the output current and voltage of the solar PV panel is

$$\left.\frac{di_p}{dv_1}\right|_{\check{v}_1,\check{i}_p} = -\frac{\check{i}_p}{\check{v}_1} \tag{3}$$

This operating point is shown in Fig. 2 with $\check{v}_1$ and $\check{i}_p$. In the conventional method, a DC/DC boost converter is connected to the output of the solar PV panel for tracking the MPP. However, like other energy conversion systems, a stability margin is required to achieve dynamic stability in a solar PV panel athigh level loading close to the MPP.

Another component of the DC microgrid is the battery. A battery plays an important role in operating an IDCM for power balancing between solar PV panels and demand. The battery can be modeled in experimental, electrochemical, and equivalent circuits. For dynamic modeling of an IDCM, a circuit model with the voltage source (E) and series resistance (r) is more appropriate. A DC/DC bidirectional buck-boost converter is connected between the battery and the DC-link capacitor to adjust the DC-link voltage to the desired values. When the output power of the solar PV panel exceeds the load, the battery absorbs and stores the extra power from the PV panel. Also, if the solar PV panel cannot meet the requested power of the load, the current is injected from the battery to the DC link to adjust the DC-link voltage.

Fig. 3 shows the IDCM-integrated circuit model. The structure of this IDCM includes a solar PV panel, a DC/DC boost converter between the solar PV panel and DC-link capacitor, a battery, a DC/DC bidirectional buck-boost converter between the battery and DC-link capacitor, a constant resistance load (R_1), a current source (i_{dc}) parallel connected to the DC-link node, and a DC/DC buck converter with CPL connected to the DC-link capacitor from a long transmission line (R_L). The power demand of the CPL is given as P_L. The switching control signal of the boost converter (q_1) is adjusted by pulsewidth modulation (PWM) to regulate the output power of the solar PV panel. Also, the switching control signal of the buck/boost converter (q_2) is adjusted by PWM for tuning the DC-link voltage and controlling the charge and discharge of the battery. Finally, the switching control signal of the buck converter (q_3) regulates the CPL voltage.

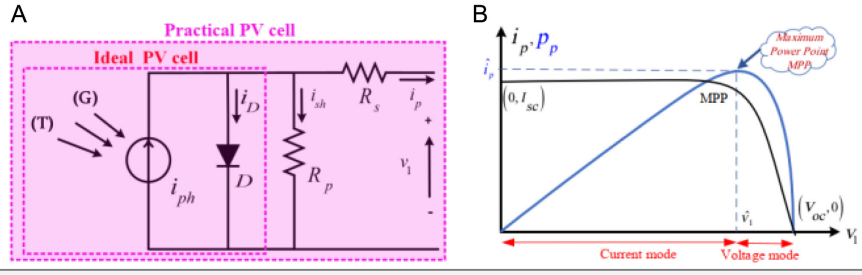

Fig. 2. Solar photovoltaic panel with characteristics.

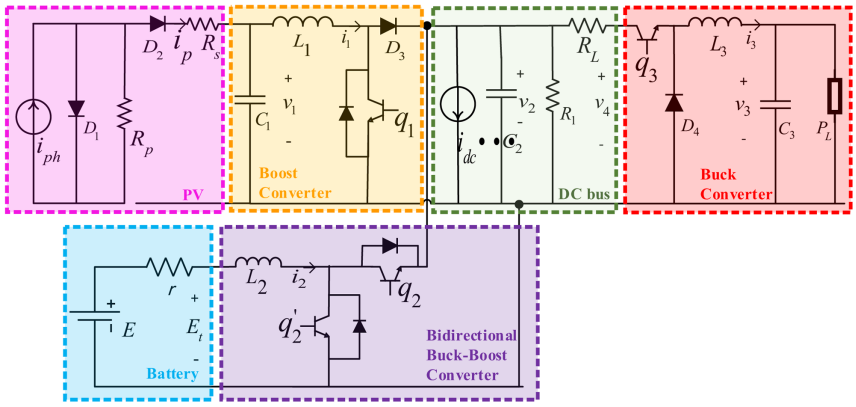

Fig. 3. Integrated configuration of the isolated direct current microgrid with solar photovoltaic panel.

III. DYNAMICAL MODEL OF THE ISOLATED DIRECT CURRENT MICROGRID

For analysis of the IDCM in Fig. 3, the state-space model of the system can be determined by applying voltage and current balance relations in inductor loops and capacitive nodes. The state-space model in the average value can be written as

$$\begin{aligned}
C_1\frac{dv_1}{dt} &= i_{ph} - I_o\left(e^{\alpha(v_1+R_s i_1)}-1\right) - \frac{v_1+R_s i_1}{R_p} - i_1 \\
L_1\frac{di_1}{dt} &= v_1 - v_2(1-d_1) \\
C_2\frac{dv_2}{dt} &= i_1(1-d_1) + i_2 d_2 - \frac{v_2}{R_1} - i_3 d_3 - i_{dc} \\
L_2\frac{di_2}{dt} &= E - i_2 r - v_2 d_2 \\
C_3\frac{dv_3}{dt} &= i_3 - \frac{P_L}{v_3} \\
L_3\frac{di_3}{dt} &= (v_2 - i_3 R_L)d_3 - v_3
\end{aligned} \tag{4}$$

where i_1, i_2, and i_3, are the average values of the inductor currents of the boost, buck-boost, and buck converters, respectively. Also, v_1, v_2, and v_3 are the average values of the capacitor voltages of the boost, buck-boost, and buck converters, respectively. The switching control signals of these converters are $q_i = \{0,1\}, i = 1,2 \text{and} 3$, and their average values are duty cycle signals with the following constraints.

$$0 \le d_i \le 1, \text{for} i = 1,2,3 \tag{5}$$

For operating a solar PV panel in the MPP, the DC input voltage of the boost converter is adjusted by the d_1 control command. Also, in the buck converter with the CPLs, the DC output voltage is regulated by the d_3 control command. A classical or nonlinear controller in a centralized structure is usually implemented in the IDCM. Classic controllers, such as proportional integral (PI) or PI derivative (PID), have a simple structure and eliminate steady-state error. However, due to the nonlinearity of the IDCM, classical approaches for designing these controllers, especially with CPLs, do not have acceptable results. In the following, a new technique for designing the decentralized controllers for the nonlinear state-space model of an IDCM is introduced.

IV. VOLTAGE CONTROL IN THE BUCK CONVERTER WITH CONSTANT POWER LOAD

Due to the CPL in the buck converter, a stabilizer should first be considered for this converter. Therefore, an inner-loop controller is considered to stabilize the closed loop system and an outer-loop controller is applied to regulate the output voltage of the converter. Regarding Fig. 3, the dynamic model of the buck converterwith CPL is

$$L_3\frac{di_3}{dt} = v_4 d_3 - v_3 \tag{6}$$

$$C_3\frac{dv_3}{dt} = i_3 - \frac{P_L}{v_3} \tag{7}$$

where v_4 is the input voltage of this converter. By replacing the capacitor voltage in (7) by the capacitor energy $\left(w_3 = \frac{1}{2}C_3 v_3^2\right)$, we have.

$$\frac{dw_3}{dt} = w_e - P_L \tag{8}$$

where $w_e = i_3 v_3$ and using the linearizer feedback technique at the control input, (6) can be written as

$$\frac{dw_e}{dt} = \frac{1}{L_3}\left(u_3 - \frac{2w_3}{C_3}\right) \tag{9}$$

$$u_3 = v_3 v_4 d_3 + \frac{L_3}{C_3}(i_3 - i_L)i_3 \tag{10}$$

where i_L is the load current. The state-space model (8) to (10) illustrates an energy model of the buck converter with CPL. This model is converted to a linear system based on the energy variables in the form of an open-loop system.

The input control of this model is u_3, and i_L is considered a disturbance. The state vector of this system is also considered $x_3 = [w_3 w_e]^T$. The eigenvalues of the open-loop system have pure complex roots, so this system has oscillating behavior. A cascade closed-loop system can be considered to track the voltage (or w_3) to the desired

reference values (w_{3r}). The internal loop provides system stability with a fixed gain (k_{p1}), and the outer loop is considered an integral controller for tracking the output voltage of the buck converter without any steady-state error. If in (10), $u_3 = k_{p1}(w_{er} - w_e)$, we have

$$\frac{dw_e}{dt} = \frac{1}{L_3}\left(k_{p1}w_{er} - \frac{2}{C_3}w_3 - k_{p1}w_e\right) \tag{11}$$

The system eigenvalues (8) and (11) are

$$\lambda_{1,2} = -\frac{k_{p1}}{L_3} \pm \sqrt{\frac{k_{p1}^2}{L_3^2} - \frac{8}{L_3C_3}} \tag{12}$$

Therefore, for $k_{p1} = 2\sqrt{L_3/C_3}$, the complex eigenvalues of the system are stable. The real and imaginary parts of these eigenvalues are the same. In this case, the damping coefficient factor of the closed loop of the buck converter with CPL is $\xi = 0.707$. An integrator with gain k_{i1} is also used to track the storage energy of the capacitor w_3 to the reference values of w_{3r}. In this case, the state-space model of the closed-loop system is.

$$\frac{d}{dt}\begin{bmatrix} w_3 \\ w_e \\ e_{w3} \end{bmatrix} = \begin{bmatrix} 0 & 1 & 0 \\ \frac{-2}{L_3C_3} & \frac{-k_{p1}}{L_3C_3} & \frac{k_{p1}k_{i1}}{L_3} \\ -1 & 0 & 0 \end{bmatrix}\begin{bmatrix} w_3 \\ w_e \\ e_{w3} \end{bmatrix} + \begin{bmatrix} 0 & -1 \\ 0 & 0 \\ 1 & 0 \end{bmatrix}\begin{bmatrix} w_{3r} \\ P_L \end{bmatrix} \tag{13}$$

where e_{w3} shows the integrator output of the capacitor energy error for C_3. The characteristic equation of this system is

$$\Delta(s) = L_3C_3s^3 + C_3k_{p1}s^2 + 2s + C_3k_{p1}k_{i1} \tag{14}$$

As a result, according to the Routh–Hurwitz stability criterion, the stability condition of this system can be obtained.

$$k_{p1} > 0, k_{i1} < \frac{2}{L_3C_3} \tag{15}$$

Therefore, for $k_{p1} = 2\sqrt{L_3/C_3}$ and $k_{i1} < 2/(L_3C_3)$, the buck converter with CPL is a stable system with zero steady-state error. The detailed structure of this controller is shown in Fig. 4. This structure represents a decentralized controller because all the necessary signals to adjust the duty cycle of the buck converter are received from the input and output terminals of the converter. This controller provides internal stability with zero steady-state error in regulating the output voltage of the CPL.

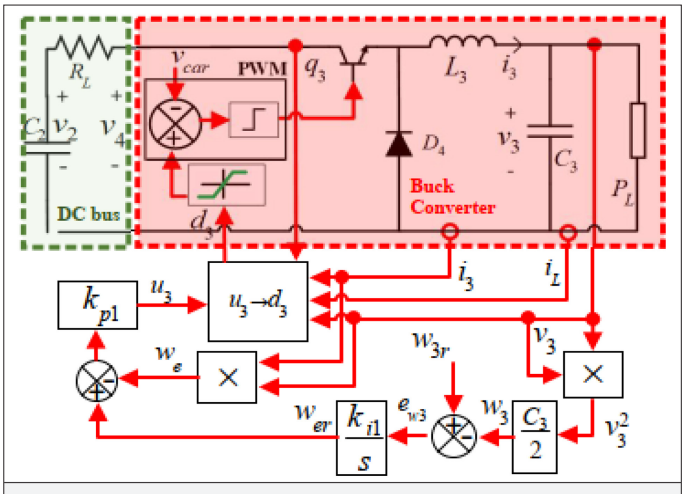

Fig. 4. The proposed controller for the buck converter.

V. MAXIMUM POWER POINT TRACKING CONTROL IN THE BOOST CONVERTER

A feedback linearization technique is applied to the boost converter to regulate the output power of the solar PV panel for operation on the MPP condition. For this purpose, the inductor current of the boost converter is adjusted to $i_{1r} = P_p / v_1$; therein after, the output power of the solar PV panel can follow the MPP. Also, according to the characteristics of the solar PV panel in Fig. 1, the output voltage and power of the solar PV panel can be followed by the MPP. The voltage and current of solar PV panels under MPP are denoted by $\check{v}_1$ and $\check{i}_1$, respectively. For this purpose, the dynamic model of the boost converter, according to Fig. 3, is

$$L_1\frac{di_1}{dt} = v_1 - u_1' \tag{16}$$

$$C_1\frac{dv_1}{dt} = \frac{P_p}{v_1} - i_1 \tag{17}$$

where $P_p = \check{v}_1\check{i}_1$ is the desired output power of the solar PV panel from MPPT unit, and $u_1' = v_2d_1'$ is considered as control input. For tracking control with zero steady-state error, a proportional and integral controller is used in the closed-loop system. The output of this controller is given by

$$u_1' = -k_{p2}(i_{1r} - i_1) - k_{i2}e_1 \tag{18}$$

where i_{1r} is the reference current of the boost inductor for absorption P_p from the solar PV panel under any operation conditions. For tracking with zero steady-state error, the output of the integrator (e_1) is considered as

$$\frac{de_1}{dt} = i_{1r} - i_1 \tag{19}$$

By combining (17) with (19), we have

$$u_1' = -k_{p2}C_1\frac{dv_1}{dt} - k_{i2}C_1v_1 \tag{20}$$

Also, by substituting (20) into (16), we can obtain

$$L_1\frac{di_1}{dt} = v_1 + k_{p2}C_1\frac{dv_1}{dt} + k_{i2}C_1v_1 \tag{21}$$

Relations (17) and (21) show a nonlinear dynamic model of the closed-loop boost converter for regulating the output power of the solar PV panel. To determine the parameters of the controller, it is necessary to apply Lyapunov's stability theorem for guaranteeing stability of the nonlinear system. For this purpose, a deviated model of capacitor voltage in (P_p), we can write.

$$P_p\left(\frac{1}{v_1} - \frac{1}{\check{v}_1}\right) = -\frac{P_p}{\check{v}_1v_1}\tilde{v}_1 = -a(t)\tilde{v}_1 \tag{22}$$

where $\tilde{v}_1 = v_1 - \check{v}_1$ is deviation of the PV output voltage from $\check{v}_1$. Under any operation conditions of the solar PV panel, the output voltage and power are positive ($v_1 > 0 \& P_p > 0$). Also, the amplitude of the output voltage deviation of the solar PV panel is lower than $\check{v}_1$ (i.e. $|\tilde{v}_1| < \check{v}_1$). Thus, for a given output power of the solar PV panel, $a(t)$ in (22) is a positive term; therefore, by combining (17) and (22), the dynamic model of the PV output voltage in deviation form can be determined as

$$C_1 \frac{d\tilde{v}_1}{dt} = -a(t)\tilde{v}_1 - \tilde{i}_1, a(t) > 0 \tag{23}$$

in which $\tilde{i}_1 = i_1 - \check{i}_1$. Also, by combining (21) with (23) based on the deviation variables, we have

$$L_1 \frac{d\tilde{i}_1}{dt} = \left(1 - a(t)k_{p2} + k_{i2}C_1\right)\tilde{v}_1 - k_{p2}\tilde{i}_1 \tag{24}$$

For evaluating the system stability in (23) and (24), the energy function is given by

$$\varepsilon = \frac{1}{2}C_1\tilde{v}_1^2 + \frac{1}{2}L_1\tilde{i}_1^2 \tag{25}$$

Using (23) to (25), the time rate of the energy function can be determined by

$$\dot{\varepsilon} = -a(t)\tilde{v}_1^2 + \left(-a(t)k_{p2} + k_{i2}C_1\right)\tilde{v}_1\tilde{i}_1 - k_{p2}\tilde{i}_1^2 \tag{26}$$

For the system stability, the sign of the $\dot{\varepsilon}$ should be negative. To achieve this result, we can consider

$$-a(t)k_{p2} + k_{i2}C_1 = 0 \tag{27}$$

On the other hand, by changing the radiation of the solar PV panel at $t = 0$, the output power of the solar PV panel changes from P_p to $P_p + \Delta P_p$ by MPPT unit. Since the inductor current and capacitor voltage in the boost converter are continuous signals, so $\tilde{i}_1(0^+) = 0$ and $v_1(0^+) = v_1(0^-) \approx \check{v}_1$. Thus, according to (17) and (20), we have

$$\tilde{u}_1'(0^+) = k_{p2}\frac{\Delta P_p}{\check{v}_1} \tag{28}$$

On the other hand, the DC-link voltage is independently adjusted by the buck-boost converter to v_{2r}. Therefore, the DC-link voltage does not change at the moment of changes in the power input by the solar PV panel (i.e. $v_2(0^+) = v_2(0^-) = v_{2r}$). Regarding $u_1' = v_2 d_1'$, the deviation of the duty cycle at $t = 0^+$ is $\tilde{d}_1'(0^+) = \tilde{u}_1(0^+)/v_{2r}$.

Thus, for the worst-case condition, the maximum variations of the duty cycle of the boost converter $t = 0^+$ are

$$\max \tilde{d}_1'(0^+) = \frac{k_{p2}\max|\Delta P_p|}{\check{v}_1 v_{2r}} \tag{29}$$

In addition, according to the constraints in (5) $\left(0 \le d_1'(t) \le 1\right)$ and the boost converter gain $\left(d_1' = \check{v}_1 / v_{2r}\right)$, the maximum variations $\tilde{d}_1'(0^+)$ can be written as

$$\max \tilde{d}_1'(0^+) = \min\left(1 - \frac{\check{v}_1}{v_{2r}}, \frac{\check{v}_1}{v_{2r}}\right) \tag{30}$$

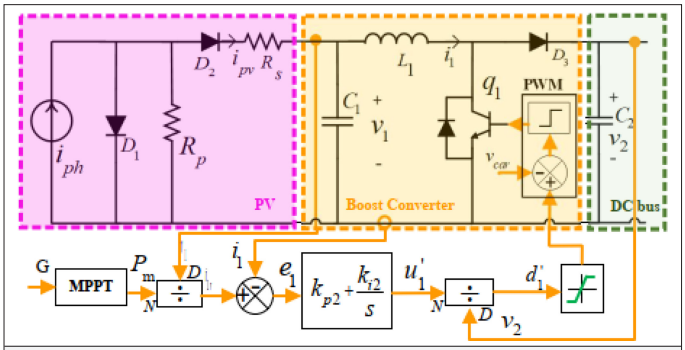

Fig. 5. Block diagrams of the proposed controllers for the boost converter.

Therefore, by combining (29) and (30), we have

$$k_{p2} \le \frac{\check{v}_1 v_{2r}}{\max|\Delta P_p|}\min\left(1 - \frac{\check{v}_1}{v_{2r}}, \frac{\check{v}_1}{v_{2r}}\right) \tag{31}$$

The upper bound of integrator gain (k_{i2}) is also obtained from (27) and (31) as

$$k_{i2} \le \frac{P_p}{C_1 \max|\Delta P_p|} \tag{32}$$

Using (31) and (32), the coefficients k_{p2} and k_{i2} can be determined in the boost converter. Fig. 5 shows the block diagram of this controller. This structure represents a decentralized controller because all the necessary signals to adjust the duty cycle of the boost converter are received from the input and output terminals of the converter. Also, the closed-loop system has internal stability with zero steady-state error for MPPT in the solar PV panel.

VI. DIRECT CURRENT-LINK VOLTAGE CONTROL IN THE BUCK-BOOST CONVERTER

In order to balance the power injected by the solar PV panel and the power absorbed by the CPL load, it is necessary to use an energy storage source such as a battery. By connecting a bilateral buck-boost converter between the DC-link and the battery, the DC-link voltage can be adjusted independently. The dynamic relation for the inductor current of the buck-boost converter in Fig. (3) can be written as

$$L_2 \frac{di_2}{dt} = E - i_2 r - u_2, u_2 = v_2 d_2 \tag{33}$$

In this model, r is the internal resistance of the battery and its value is small. This resistance helps to damp the oscillations of the buck-boost converters' variables. Therefore, the design of the controller parameters by ignoring this resistance will lead to more suitable results in the stability of the real system. For stabilizing the DC-link voltage, current and voltage controllers are considered in the cascade connection. A current controller is applied for tracking the inductor current in the internal loop. A voltage controller is considered for DC-link voltage regulation in the outer loop. For the current controller in the internal loop, we can write

$$u_2 = -k_{p3}\left(i_{2r} - i_2\right) - k_{i3}e_2 \tag{34}$$

$$\frac{de_2}{dt}=i_{2r}-i_2 \tag{35}$$

where k_{p3}, and k_{i3} are the gains of the current controller, and e_2 is the integrator output of the current regulator. Also, i_{2r} is the reference current of the buck-boost inductor. The DC-link voltage controller generates i_{2r}. The characteristic equation of the system (33) and (35) based on the i_{2r} as input and i_2 as output is.

$$\Delta(s)=s^2+k_{p3}s+k_{i3} \tag{36}$$

Therefore, by selecting k_{p3} and k_{i3}, the natural frequencies of the current control can be adjusted. To obtain a coefficient damping factor of $\xi=0.707$, we can write.

$$k_{i3}=\frac{k_{p3}^2}{2} \tag{37}$$

The proportional gain k_{p3} can also be adjusted based on the maximum duty cycle of the buck-boost converter, similar to the boost converter in the previous section. By selecting a large gain for k_{p3}, the natural frequency of the current controller is significantly increased, and as a result the transient response of the current regulating i_2 to i_{2r} is significantly decreased (i.e. $i_2\cong i_{2r}$). In this condition, using (33) and $i_{2r}/dt\cong 0$, we have

$$d_2\cong\frac{E_t}{v_2},E_t=E-ri_{2r} \tag{38}$$

where E_t is the battery terminal voltage. On the other hand, by combining (4) and (38), the dynamics of the capacitor voltage are obtained as

$$C_2\frac{dv_2}{dt}=i_1d_1^{'}+i_{2r}d_2-\frac{v_2}{R_1}-i_3d_3 \tag{39}$$

If the difference between the injection current of the solar PV panel and the input current of the buck converter is considered as an external constant perturbation applied to the DC link, then, by combining (38) and (39), we have

$$\frac{dw_2}{dt}=-\frac{2w_2}{C_2R_1}+u_4+\delta P,u_4=i_{2r}E_t \tag{40}$$

where w_2 is the energy stored in capacitor C_2 and δP expresses the power perturbation due to the power injected by the solar PV panel and the power absorbed by the R_1, i_{dc}, and CPL. Also, u_4 is the output control for the DC-link voltage controller. For a closed-loop control of the DC-link voltage with a PI compensator, the reference current i_{2r} can be determined as

$$i_{2r}=\frac{1}{E_t}\left(k_{p4}\left(w_{2r}-w_2\right)+k_{i4}e_{w2}\right) \tag{41}$$

$$\frac{de_{w2}}{dt}=w_{2r}-w_2 \tag{42}$$

where e_{w2} indicates the output signal of the integrator, and k_{p4} and k_{i4} are gains of the DC-link voltage controller. Also, w_{2r} is the reference value of energy storage in the DC-link capacitor ($w_{2r}=C_2v_{2r}^2/2$). As a result, the characteristic equation of the closed-loop system (40) and (42) is

$$\Delta(s)=s^2+\left(\frac{2}{C_2R_1}+k_{p4}\right)s+k_{i4} \tag{43}$$

In this case, k_{p4} it k_{i4} can be determined for system stability based on the maximum allowable i_{2r} and the proper damping factor of the closed-loop system. Finally, using (33), (34), (40), and (41) we have

$$i_{2r}=\frac{1}{E_t}\left(k_{p4}\left(w_{2r}-w_2\right)+k_{i4}e_{w2}\right) \tag{44}$$

$$d_2=\frac{1}{v_2}\left(-k_{p3}\left(i_{2r}-i_2\right)-k_{i3}e_2\right) \tag{45}$$

The closed-loop model of the system based on these controllers is shown in Fig. 6. The integrated model of the DC microgrid with the decentralized controller is depicted in Fig. 7.

VII. SIMULATION RESULTS

Simulation studies are performed in various conditions with significant changes in radiation and output load to evaluate the performance of the proposed closed-loop system. Also, in order to compare the results of the proposed method with other references, the parameters of the system provided in [18] have been used. These parameters are listed in Table II. The DC-link reference voltage is given as 120 volts, and the CPL output voltage is considered to be 28 volts. The parameters of the controllers are illustrated in Table III based on the design techniques in the previous section.

For simulation studies, the DC microgrid is considered in the steady-state at $t=0$. The output load of the buck converter is also given zero at $t=0$. The variations of the output power of the solar PV panel (P_p), and CPL (P_L) are illustrated in Figs. 8 and 9. For example, during $0<t<20$ ms, the photocurrent is 9 A with the solar radiation $G=900\text{W}/\text{m}^2$. The output power of the solar PV panel should be set to 267.5 W with MPPT unit.

Fig. 8 shows the dynamic performances of i_1,v_1,p_1, and $d_1^{'}$ with the proposed controllers. In this figure, the extra graphs in light color show the system variables in switching conditions with some ripples. The fast regulation of the capacitor voltage in the boost converter is

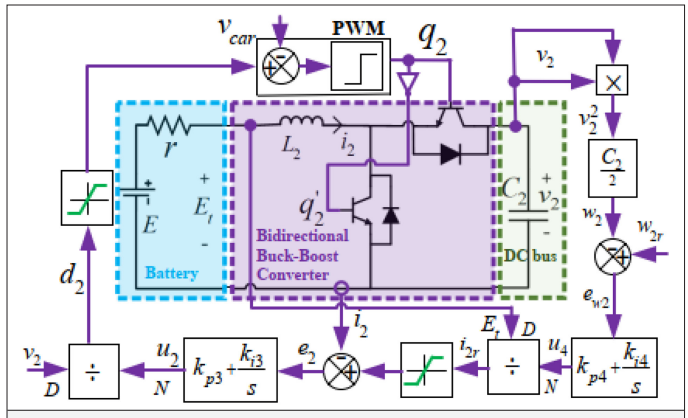

Fig. 6. Block diagrams of the proposed controllers for the buck-boost converter.

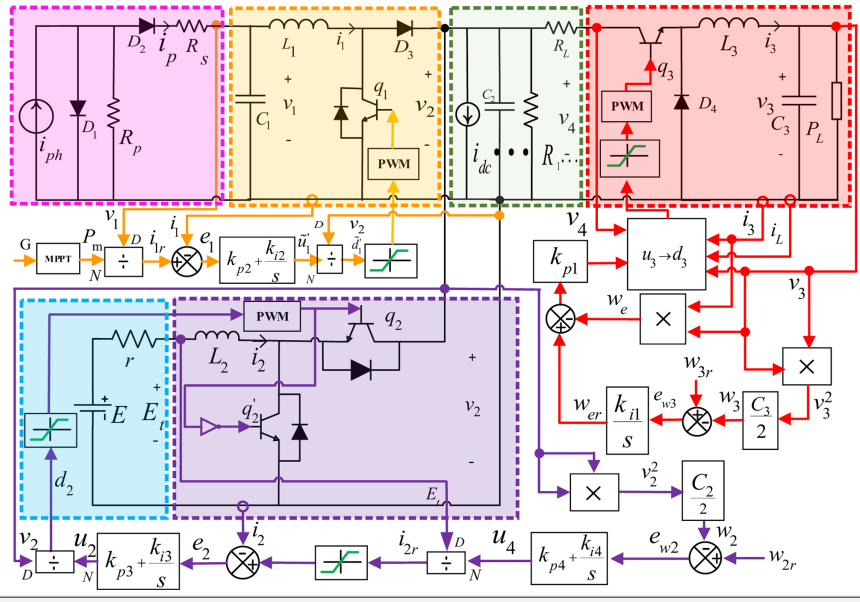

Fig. 7. The block diagram of the integrated model of the DC microgrid with the proposed controllers.

TABLE II. THE DC-MICROGRID PARAMETERS

Parameters	Values	Parameters	Values
L_1	5 mH	r	1 Ω
L_2	5 mH	R_p	$10^6\,\Omega$
L_3	5 mH	R_L	10 Ω
C_1	200 μ F	E	48 V
C_2	2000 μ F	Q	1.6×10^{-19}
C_3	300 μ F	K	1.38×10^{-23}
R_1	144 Ω	N_s	65
P_L	87 W	T	48
I_o	10^{-9} A	R_s	0.01 Ω
I_{pvn}	8.66 A	α	0.555

TABLE III. THE CONTROLLER PARAMETERS

Proportional Gains	Integral Gains
$k_{p1}=2\sqrt{\frac{L_3}{C_3}}=10\sqrt{\frac{2}{3}}$	$k_{i1}=\frac{0.25}{L_3C_3}=1.67\times10^5$
$k_{p2}=150$	$k_{i2}=10^4$
$k_{p3}=50$	$k_{i3}=k_{p3}^2/2=1250$
$k_{p4}=1100$	$k_{i4}=3\times10^5\le k_{p4}^2/2$

shown in this figure. At $t=40$ ms, due to the lack of solar radiation and the presence of a capacitor in the boost converter, the output voltage of the solar PV panel slowly begins to decrease. In addition, Fig. 9 shows the dynamic performances of i_2, v_2, p_2, and d_2.

The maximum currents of the charge/discharge of the battery are limited to 8 A. This limitation occurs at 20 ms. When the radiation is $G=900\text{w}/\text{m}^2$, the battery current is negative, i.e., the converter is in buck mode, and therefore the battery is also in charge mode. By reducing the radiation on the $20\le t\le60$ ms, the converter operates

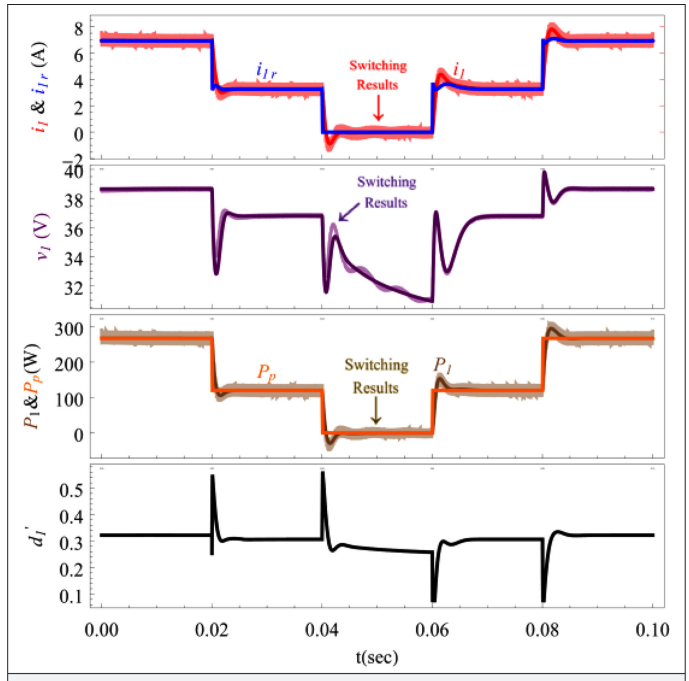

Fig. 8. Dynamic performances of the system variables (i_1, v_1, P_1 & d_1') with the proposed controllers.

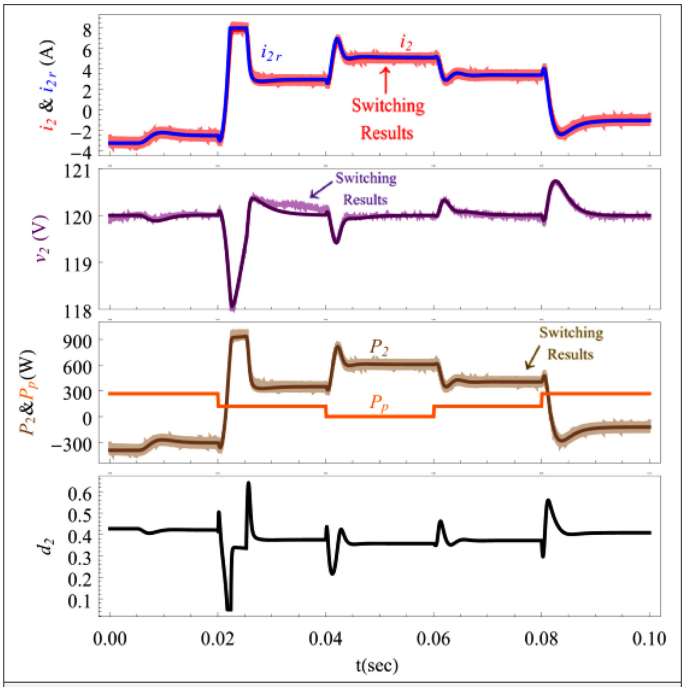

Fig. 9. Dynamic performances of the system variables (i_2, v_2, p_2, P_p & d_2) with the proposed controllers.

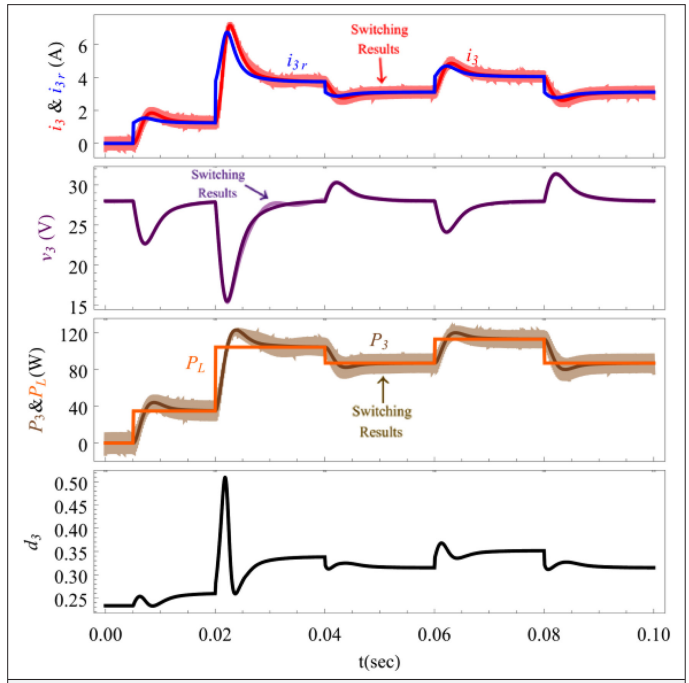

Fig. 10. Dynamic performances of the system variables (i_3, v_3, p_3, P_L & d_3) with the proposed controllers.

in boost mode, and therefore, the battery is discharged to adjust the DC-link voltage with a stable response.

Fig. 10 shows the dynamic performances of i_3, v_3, p_3, and d_3 with the proposed controller. The current from zero (under no load) quickly increased to reference values by changing the CPL in the output of the buck converter. The fast and desirable dynamic response under different operating conditions can be seen for regulating the CPL voltage by the proposed controller. In Fig. 11, the power–voltage and current–voltage trajectories of the solar PV panel are illustrated. For instance, the trajectories of the solar PV panel move from the radiation $G = 900\text{W} / \text{m}^2$ with the dynamical MPP $P_p = 267.5$ W to $G = 400\text{W} / \text{m}^2$ with $P_p = 120$ W.

Generally, the parallel connection of a linear resistor, current source, and constant power load to the DC link in an IDCM is considered as a nonlinear load [25]. To evaluate the dynamical performance of the system in this condition, a parallel current source (i_{dc}) is connected to the DC link. The results in Fig. 9 are repeated when a square waveform of a current source with an amplitude of 0.9 A is connected to the DC link. The simulation results for buck and boost converters are similar to the previous simulation result in Figs. 8 and 10; however, simulation results for buck-boost converters are depicted in Fig. 12. This figure shows that the DC-link voltage is stable by duty cycle control of the buck-boost converter, but the voltage ripple of the DC-link capacitor is increased a little. It is clear that the increase in voltage ripple is due to the square waveform of the DC current source, which is generally reduced by choosing the appropriate capacity of the D-link capacitor, and it does not depend on the controller.

In Fig. 11, the power–voltage and current–voltage trajectories of the solar PV panel are illustrated. For instance, the trajectories of the solar PV panel move from the radiation $G = 900\text{W} / \text{m}^2$ with the dynamical MPP $P_p = 267.5$ W to $G = 400\text{W} / \text{m}^2$ with $P_p = 120$ W.

The passivity-based and conventional PI controllers are implemented to create a base for comparison. For evaluating the response of the closed-loop system with proposed controllers, the simulation

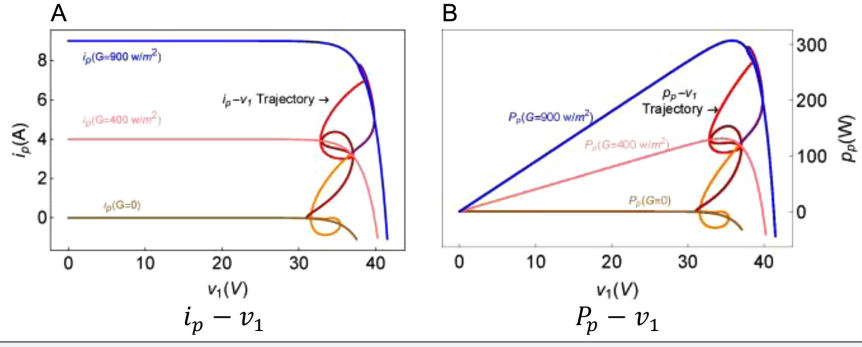

Fig. 11. Trajectories of the solar photovoltaic panel for Maximum Power Point Tracking.

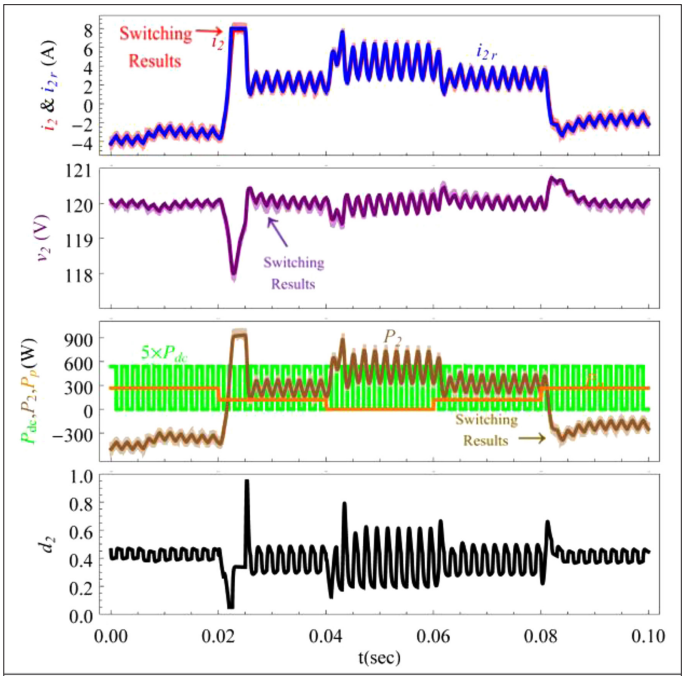

Fig. 12. Dynamic performances of the system variables (i_2, v_2, p_2, P_p & d_2) with the proposed controllers with parallel connected current source and constant power load to DC link.

analysis based on the passivity-based control method presented in [18] is shown in Fig. 13. All simulation conditions are the same as in previous simulations. In this figure, the desired performances of the proposed controllers are compared to passivity-based and classical PI control. At $t=20$ ms, the radiation decreases from 900 to 400 W/m^2 and at $t=80$ ms, it increases to 900 W/m^2. These changes

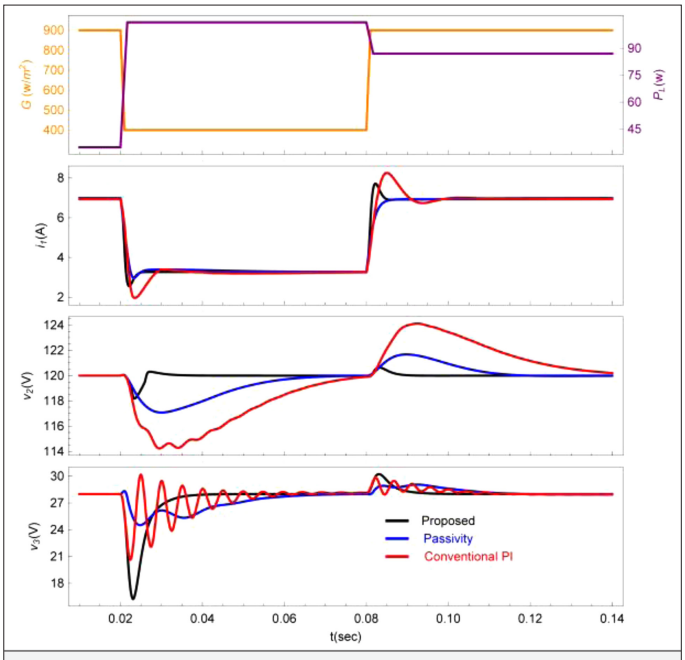

Fig. 13. Comparison of the proposed (black), passivity-based (blue), and traditional PI (red) controllers under different CPL (orange) and radiation (purple) conditions.

in radiation cause the output power of the solar PV panel to vary between 267.5 and 120 W. On the other hand, CPL increases from 34.8 to 104.4 W at $t=20$ ms and decreases to 87 W at $t=80$ ms. The output current of the solar PV panel, the DC-link voltage, and the output voltage of the buck converter are shown in Fig. 13.

Despite the changes in load and solar radiation, the proposed controllers quickly regulated the DC-link voltage to the reference values. It is observed that the system's response under classical PI controllers is oscillatory.

VIII. CONCLUSION

In this paper, a DC microgrid including the buck, boost, and buck-boost converters was introduced, and decentralized controllers were designed and implemented using the feedback linearization technique. There was no need for communication infrastructure in the decentralized linearization control system. The results were presented under conventional, passivity, and proposed controllers for different environmental conditions, and a comparison was made between them. The results show that the proposed controller had faster dynamic performance than the passivity and other classical controllers.

Peer-review: Externally peer-reviewed.

Author Contributions: Concept – J.N.; Design – H.A., J.N.; Supervision – J.N.; Funding – J.N.; Materials – H.A., J.N.; Data Collection and/or Processing – H.A.; Analysis and/or Interpretation – H.A., J.N.; Literature Review – H.A.; Writing – H.A., J.N.; Critical Review – J.N.

Declaration of Interests: The authors have no conflict of interest to declare.

Funding: The authors declared that this study has received no financial support.

REFERENCES

1. J. Kumar, A. Agarwal, and N. Singh, "Multipurpose water storage tank based DC microgrid system for isolated communities," *Energy Storage*, vol. 4, no. 4, p. e308, 2022. [CrossRef]
2. S. K. Singh, A. Agarwal, and T. Kanumuri, "Power quality improvement of a fuel cell-powered filterless distributed generation system using sinusoidal pulse width modulation," *Indian J. Pure Appl. Phys. (IJPAP)*, vol. 60, no. 9, pp. 754–762, 2022. [CrossRef]
3. M. Salehi, S. A. Taher, I. Sadeghkhani, and M. Shahidehpour, "A poverty severity index-based protection strategy for ring-bus low-voltage DC microgrids," *IEEE Trans. Smart Grid*, vol. 10, no. 6, pp. 6860–6869, 2019. [CrossRef]
4. G. Sahoo, R. K. Sahu, P. C. Pradhan, and S. Panda, "Design and analysis of enhanced Harris Hawks optimization-tuned Type-2 fuzzy fractional proportional integral derivative controller for the frequency control of microgrid system," *ELECTRICA*, vol. 1, no. 1, pp. 1–7, 2022. [CrossRef]
5. E. Ganesan, S. S. Dash, and C. Samanta, "Modeling, control, and power management for a grid-integrated photo voltaic, fuel cell, and wind hybrid system," *Turk J. Elec Eng & Comp Sci*, vol. 24, no. 6, pp. 4804–4823, 2016. [CrossRef]
6. J. Kumar, A. Agarwal, and N. Singh, "A decentralised power management strategy in a hybrid energy storage supported islanded residential sustainable DC microgrid system," *Int. J. Energy Technol. Policy*, vol. 18, no. 1, pp. 1–31, 2022. [CrossRef]
7. J. Li, H. Pan, X. Long, and B. Liu, "Objective holographic feedbacks linearization control for boost converter with constant power load," *Int. J. Electr. Power Energy Syst.*, vol. 134, p. 107310, 2022. [CrossRef]
8. B. B. ALAGÖZ, C. KELEŞ, A. Kaygusuz, Y. Kaplan, and A. K. KARABİBER, "Power regulated DC/DC driver design by hierarchical control," *Turk J. Elec Eng & Comp Sci*, vol. 24, no. 3, pp. 1325–1339, 2016. [CrossRef]

9. C. Liu, J. Zhao, S. Wang, W. Lu, and K. Qu, "Active identification method for line resistance in DC microgrid based on single pulse injection," *IEEE Trans. Power Electron.*, vol. 33, no. 7, pp. 5561–5564, 2017. [CrossRef]
10. Y. Han, X. Ning, P. Yang, and L. Xu, "Review of power sharing, voltage restoration and stabilization techniques in hierarchical controlled DC microgrids," *IEEE Access*, vol. 7, pp. 149202–149223, 2019. [CrossRef]
11. S. M. Said, A. Ali, and B. Hartmann, "Tie-line power flow control method for grid-connected microgrids with SMES based on optimization and fuzzy logic," *J. Mod. Power Syst. Clean Energy*, vol. 8, no. 5, pp. 941–950, 2020. [CrossRef]
12. A. Iovine, S. B. Siad, G. Damm, E. De Santis, and M. D. Di Benedetto, "Nonlinear control of a DC microgrid for the integration of photovoltaic panels," *IEEE Trans. Autom. Sci. Eng.*, vol. 14, no. 2, pp. 524–535, 2017. [CrossRef]
13. I. Rai, R. Anand, A. Lashab, and J. M. Guerrero, "Hardy space nonlinear controller design for DC microgrid with constant power loads," *Int. J. Electr. Power Energy Syst.*, vol. 133, p. 107300, 2021. [CrossRef]
14. P. Li, T. Guo, F. Zhou, J. Yang, and Y. Liu, "Nonlinear coordinated control of parallel bidirectional power converters in an AC/DC hybrid microgrid," *Int. J. Electr. Power Energy Syst.*, vol. 122, p. 106208, 2020. [CrossRef]
15. V. Kumar, S. R. Mohanty, and S. Kumar, "Event trigger super twisting sliding mode control for DC micro grid with matched/unmatched disturbance observer," *IEEE Trans. Smart Grid*, vol. 11, no. 5, pp. 3837–3849, 2020. [CrossRef]
16. S. Ansari, J. Zhang, and R. E. Singh, "A review of stabilization methods for DCMG with CPL, the role of bandwidth limits and droop control," *Prot. Control Mod. Power Syst.*, vol. 7, no. 1, pp. 1–12, 2022. [CrossRef]
17. P. Lin, C. Zhang, P. Wang, and J. Xiao, "A decentralized composite controller for unified voltage control with global system large-signal stability in DC microgrids," *IEEE Trans. Smart Grid*, vol. 10, no. 5, pp. 5075–5091, 2018. [CrossRef]
18. J. Sun, W. Lin, M. Hong, and K. A. Loparo, "Voltage regulation of DC-microgrid with PV and battery," *IEEE Trans. Smart Grid*, vol. 11, no. 6, pp. 4662–4675, 2020. [CrossRef]
19. W. Lin, "Feedback stabilization of general nonlinear control systems: A passive system approach," *Syst. Control Lett.*, vol. 25, no. 1, pp. 41–52, 1995. [CrossRef]
20. W. Lin, "Global asymptotic stabilization of general nonlinear systems with stable free dynamics via passivity and bounded feedback," *Automatica*, vol. 32, no. 6, pp. 915–924, 1996. [CrossRef]
21. H. K. Khalil, *Nonlinear Systems*, Third edn. Patience Hall, Inc. Upper Saddle River, Vol. 115, 2002. Q1
22. M. A. Hassan, E. Li, X. Li, T. Li, C. Duan, and S. Chi, "Adaptive passivity-based control of DC–DC buck power converter with constant power load in DC microgrid systems," *IEEE J Emerg Sel Top Power Electron*, vol. 7, no. 3, pp. 2029–2040, 2018. [CrossRef]
23. G. M. Vosters, and W. W. Weaver, "Energy and impedance space modeling of power electronic converters" 2011 IEEE Energy Conversion Congress and Exposition, AZ, USA, 2011, pp. 1265–1272. [CrossRef]
24. M. Mosayebi, M. Gheisarnejad, and M. H. Khooban, "An intelligent sliding mode control for stabilization of parallel converters feeding CPLs in DC-microgrid," *IET Power Electron*, vol. 15, no. 14, pp. 1596–1606, 2022. [CrossRef]
25. J. Wu, and Y. Lu, "Adaptive backstepping sliding mode control for boost converter with constant power load," *IEEE Access*, vol. 7, pp. 50797–50807, 2019. [CrossRef]
26. R. Haroun, A. A. L. Aroudi, A. Cid-Pastor, E. Vidal-Idiarte, H. Valderrama-Blavi, and L. Martinez-Salamero, Modelling and control of modular DC-nanogrids based on loss-free resistors. *IEEE Access*, vol. 8, pp. 33305–33317, 2020. [CrossRef]
27. R. Kumar, R. Kumar, and S. K. Singh, "Solar photovoltaic modeling and simulation: As a renewable energy solution," *Energy Rep.*, vol. 4, pp. 701–712, 2018. [CrossRef]

Hossein Akbari was born in Shiraz, Iran, in May 1996. He received his B.Sc degree from Persian Gulf University, Bushehr, Iran, in 2018 and his M.Sc degree from Shahed University, Tehran, Iran, in August 2021. Currently, he is joining as a senior expert in the oil and gas industry. His research interests include modeling and control of dc/dc converters, and nonlinear control techniques in microgrid systems.

Jalal Nazarzadeh was born in Tehran, in August 1964. He received his Ph.D. degree from the Amir-Kabir University of Technology, Tehran, Iran in 1998. In February 1998, he joined the Engineering Faculty, Shahed University. He is currently a full professor with the faculty of engineering. His current research interests include the modeling and control of electrical machines, power electronics converters, and nonlinear optimal control systems. Dr. Nazarzadeh is the author or co-author of several scientific papers and serves as a reviewer for several international journals.